

IDENTIFICATION OF CYCLE-TO-CYCLE VARIABILITY SOURCES IN SI ICE BASED ON CFD MODELING

OLDŘICH VÍTEK, VÍT DOLEČEK, ZBYNĚK SYROVÁTKA, JAN MACEK

Czech Technical University in Prague, Department of Automotive, Combustion Engine and Railway Engineering

Technická 4, CZ-16607 Prague 6, Czech Republic, Tel.: +420224352507, Fax: +420224352500

Email: oldrich.vitek@fs.cvut.cz, v.dolecek@fs.cvut.cz, zbynek.syrovatka@fs.cvut.cz, jan.macek@fs.cvut.cz

ABSTRACT

The presented paper deals with modelling of cycle-to-cycle variations (CCV) in SI ICEs by means of 3-D CFD LES approach. The main goals are the following: to identify the most important sources of CCV and to compare 2 different ignition systems: classical spark ignition and turbulent flame jet. Calibrated 3-D CFD LES models of these engines are applied to perform time-demanding multi-cycle calculations of selected engine operating points. The simulation data are analyzed including comparison with experimental data and main conclusions are drawn. The turbulence, which is generated during intake stroke, is identified as the main CCV source while early flame kernel development (strongly influenced by local turbulence) is also important.

KEYWORDS: LARGE EDDY SIMULATION (LES), CFD, SI ICE, CYCLE-TO-CYCLE VARIATION (CCV), MULTI-CYCLE CALCULATIONS

SHRNUTÍ

Tento článek se zabývá modelováním mezicyklové variability v zážehových spalovacích motorech pomocí 3-D CFD LES přístupu. Hlavní cíle práce jsou následující: identifikace hlavních zdrojů mezicyklové variability a porovnání 2 různých systémů pro zapálení směsi: klasický zážeh pomocí svíčky a turbulentní hořící paprsek. Kalibrované 3-D CFD LES modely těchto motorů jsou použity pro časově náročné simulace mnoha po sobě následujících cyklů pro vybrané pracovní body těchto motorů. Data ze simulací jsou analyzována včetně srovnání s experimenty a jsou formulovány hlavní závěry. Turbulence, která je primárně generována během sacího zdvihu, je identifikována jako hlavní zdroj mezicyklové variability, zatímco co úvodní fáze vývinu jádra plamene (silně ovlivněna lokální turbulencí) je taky důležitá.

KLÍČOVÁ SLOVA: SIMULACE VELKÝCH VÍRŮ (LES), CFD, ZÁŽEHOVÝ SPALOVACÍ MOTOR, MEZICYKLOVÁ VARIABILITA, SIMULACE MNOHA PO SOBĚ JDOUCÍCH CYKLŮ

1. INTRODUCTION

The operation of SI-engines is characterized by a non-repeatability of the instantaneous combustion rate of the individual engine cycles at nominally identical engine operating parameters. This phenomenon, usually referred to as cycle-to-cycle variations (CCV), strongly limits the SI-engine thermal efficiency by determining the maximum possible compression ratio and spark advance for knock-free combustion. Due to the presence of CCV, both the maximum compression ratio and spark advance is limited by the fastest burning cycle that is most prone to the onset of knock in the end-gas ahead of the flame. Hence, minimizing the cyclic dispersion of the in-cylinder combustion process for a given engine configuration offers the potential to increase engine compression ratio and to adopt the thermodynamically most efficient spark advance and

consequently to reduce the specific fuel consumption for a given power output.

A major prerequisite for the development of strategies for minimizing cycle-to-cycle combustion variations is a detailed understanding of the causes leading to the cyclic dispersion of the combustion process from one cycle to the other. Conventional cylinder pressure indication clearly provides information on the appearance of cycle-to-cycle combustion variations and also enables a quantification of the in-cylinder pressure evolution variations from one cycle to the other. However, in order to identify the origins of the cycle-to-cycle combustion variations, a detailed cycle-resolved insight into the locally governing in-cylinder flow, mixture formation and flame propagation processes including their complex mutual interactions is



required. Experimental studies allow identifying cycle-to-cycle variations for a given engine, but they are only applicable once the engine is available in hardware, i.e. in a phase of the engine development process in which modifications of the initial design are difficult to realize due to cost and time constraints.

In the above context and in view of the more and more stringent legislative demands on fuel consumption and hence CO₂ emissions, it becomes increasingly desirable to be able to predict and control individual engine cycles, and thus to address the occurrence and the impact of CCV on fuel consumption. Moreover, the ability to predict CCV in the early engine design phase is essential to exploit the full potential of promising new SI-engine technologies, such as e.g. direct-injection, downsizing, charging, etc. under real operation.

Based on above-mentioned, the main target of the presented work is to identify the main sources of cyclic variation of SI ICE operation. The other one is to compare 2 different engine cases in terms of ignition device: classical spark ignition ICE and scavenged pre-chamber gas ICE (based on [19], this engine configuration can be considered as turbulent flame jet with respect to mixture ignition process). The main tool to achieve these goals is to apply LES CFD simulation approach, which has proved to be a very efficient one when dealing with CCV phenomena in SI ICE – c.f. [1, 2, 3, 4, 5, 6, 9, 13].

2. MATHEMATICAL MODEL

For the simulation of the gas flow, spray mixture formation and flame propagation processes in the SI-engine analyzed in the present work, the 3D-CFD code AVL FIRE is adopted [22]. The 3-D CFD SW solves the general conservation equations of mass, momentum and enthalpy plus additional transport equations for turbulence related quantities and for conservation of chemical species. Depending on the physical and chemical sub-models employed, additional scalar quantities, such as e.g. mixture fraction, reaction progress variable, flame surface density, etc. are solved as well.

The adopted solution method is based on a fully conservative finite volume approach. All dependent variables, such as momentum, pressure, density, turbulence kinetic energy, dissipation rate, and the scalar quantities are evaluated at the cell centres of the general, unstructured computational grids. A second-order midpoint rule is used for integral approximation and a second order linear approximation for any value at the cell-face. Convection is solved by adopting higher order differencing schemes. In order to offer full flexibility in terms of the structure and topology of the employed computational meshes, the solver allows for each computational cell to consist of an arbitrary number of cell faces. Connectivity and interpolation practices for gradients and cell-face values are set

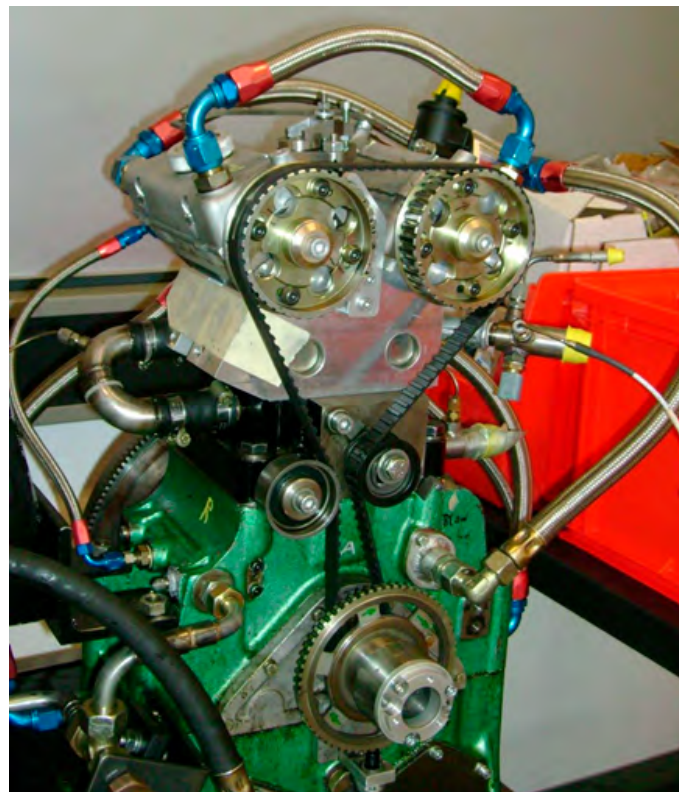


FIGURE 1: Target engine A – AVL Single Cylinder Research Engine (SI version).
OBRAZĚK 1: Cílový motor A – zkušební jednoválec od AVL (zážehová varianta).

up to accommodate such 'polyhedral' calculation volumes. The rate of change (accumulation term) is discretized by using an Euler implicit scheme. The overall solution procedure is iterative and is based on the Semi-Implicit Method for Pressure-Linked Equations algorithm (SIMPLE) or Pressure-Implicit with Splitting of Operators (PISO, c.f. [8]), applicable to turbulent flows at all speeds. For solving the large sets of linear equation systems evolving from the discretization of the governing equations, an efficient preconditioned conjugate gradient method is employed. More details can be found in [5, 6] and documentation of AVL FIRE [22].

Dealing with numerical setup, the following settings were applied. PISO algorithm was selected as time integration method while 2nd order schemes were used for convective term approximations. Time step was set to 0.1 degCA.

Regarding turbulence modelling, Large Eddy Simulation (LES) was adopted. It is based on the filtered instantaneous Navier-Stokes equations. Filtering operation actually represents scale separation in space, where large scales are directly resolved, and the influence of small scales is taken into account by the sub-grid scale (SGS) model. Smagorinsky SGS model [9, 10] was applied for the Engine A while coherent structure version of LES approach [9, 11, 12] was selected for the case of the Engine B.



Concerning combustion models, the LES version of ECFM-3Z was activated due to positive experience with this model from the past – c.f. [5, 6]. Premixed turbulent SI-engine combustion is modeled in the present case by using the LES variant of the Extended Coherent Flame Model (CFM) [13] which is based on solving a transport equation for the flame surface density (FSD), suitably linked with the gas-phase thermochemistry. It should be stressed that this model is turbulence driven, hence it cannot capture local chemical effects (e.g., flame quenching due to low temperature or turbulence-related effects) – this leads to a statement that all fuel is (usually) burnt when using this model (provided there is enough oxygen). Dealing with applied chemistry, the turbulence driven combustion models are usually linked with simplified chemistry approaches based on equilibrium. This was also the case for the presented CFD calculations. The only considered pollutant was NO_x, however its formation was based on standard approach [14], which is to solve certain equations of chemical kinetics.

The spray model adopted in the present study is based on the Lagrangian Discrete Droplet Method (DDM) [15]. In the DDM the continuous gaseous phase is described by the standard Eulerian conservation equations, whereas the transport of the dispersed phase is calculated by tracking the trajectories of representative droplet parcels. A parcel consists of a number of droplets, with all the droplets having identical physical properties and behaving equally when they move, break up, hit a wall or evaporate. The calculation of the parcel movement is done with a sub-cycling procedure between the gas phase time steps taking into account the forces exerted on the parcels by the gas phase as well as the related heat and mass transfer. The coupling between the liquid and the gaseous phases is achieved by source term exchange for mass, momentum, energy and turbulence. For the LES application, turbulent dispersion effects are assumed to be fully covered by the interaction of the droplets with the resolved LES flow field scales – hence, this term is deactivated when LES approach is applied.

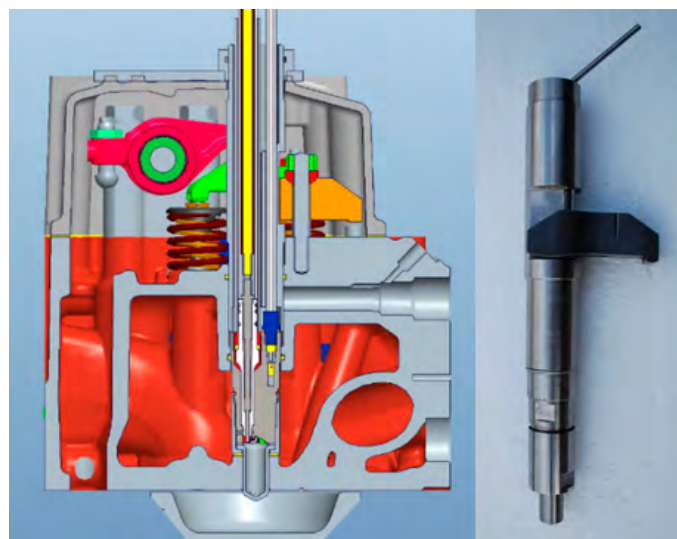
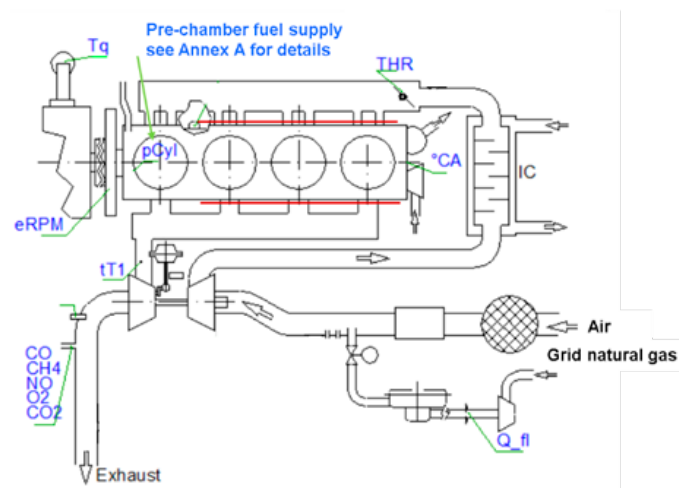


FIGURE 2: Target engine B – research engine with scavenged pre-chamber (CNG SI version).
OBRÁZEK 2: Cílový motor B – zkušební motor s vyplachovanou komůrkou (plynová zážehová varianta).

TABLE 1: Main engine parameters – version A and version B.
TABULKA 1: Hlavní parametry motoru – verze A a verze B.

Engine Parameter	Unit	Engine A	Engine B
Bore	[mm]	86	102
Stroke	[mm]	86	120
Compression Ratio	[1]	11.5	12
Charging		Naturally Aspirated	Turbocharged
Fuel		Gasoline (ON 95)	Methane
Fuel Injection		DI	PFI + pre-chamber
Number of Intake Valves		2 (phasing)	2
Number of Exhaust Valves		2 (phasing)	2



TABLE 2: Main mesh parameters for both engine version (A and B).
TABULKA 2: Hlavní parametry sítě pro obě verze motoru (A a B).

Parameter	Unit	Engine A	Engine B
Typical Mesh Size	[mm]	<1.0	<0.6
Min. Amount of Mesh Cells	[1]	1.7M	7.5M
Max. Amount of Mesh Cells	[1]	3.3M	13M
Max. Angle Interval of Single Mesh Set	[degCA]	5	10

The CFD models are based on 2 existing engine geometries (c.f. Table 1, Figure 1 and 2). 3-D CAD data of engine cylinder head, piston and liner (for both engine variants) were provided by engine manufacturers. All the necessary geometry information was available, hence the meshing procedure could be started. The meshing itself was made by means of hybrid meshing tool of AVL FIRE. Typical mesh cell size was set to 1.0 mm (the Engine A) and 0.6 mm (the Engine B) – this is based on experience from

the previous work [5, 6] with LES approach to SI ICE modeling. The important parameters of applied meshes are summarized in Table 2.

Concerning boundary and initial conditions, they were transferred from the calibrated 0-D/1-D models of the engines created in SW tools [23, 24]. To be more precise, 0-D/1-D tool [23] and 3-D CFD [22] tool were directly linked to perform fully coupled co-simulation for the case of the Engine A (c.f. Table 1) – hence, boundary conditions were provided directly by 0-D/1-D tool. For the case of the Engine B, surface temperatures were based on simplified predictive FEM model, inlet/outlet boundary pressure/temperature was imposed as function of crank angle. The same applies to fuel mass-flow rate to the pre-chamber, which represents mixture enrichment via dedicated fuel supply system. Initial values of all required thermodynamic parameters (including composition) were directly transferred from the 0-D/1-D model.

3. COMPUTED CASES

As it is mentioned above, 2 engine cases were considered (Table 1). The Engine A represents research single-cylinder DI SI ICE while the Engine B corresponds to experimental CNG SI ICE with scavenged pre-chamber. Moreover, the Engine B was heavily modified from its original version, which represents a light-duty CI ICE – hence, it is dominated by swirling in-cylinder motion while there is a significant bowl in the piston (c.f. Figure 3, lower subfigure). On the other hand, the Engine A is dominated by tumbling in-cylinder flow (c.f. Figure 3, upper subfigure). Moreover, the Engine A is equipped with direct fuel injection system – the injector is located just below intake ports ('side-mounted' configuration) and it is pointing in the same direction as a tumbling motion (created by appropriate direction of intake ports), hence supporting the in-cylinder tumble. The injection starts at early intake stroke and it takes approx. 40 degCA for considered low-IMEP cases (c.f. Table 3). The range of operating conditions related to data presented in the paper of both considered engines are summarized in Table 3. As the focus is put on CCV effects, relatively low load cases were selected to avoid knock occurrence.

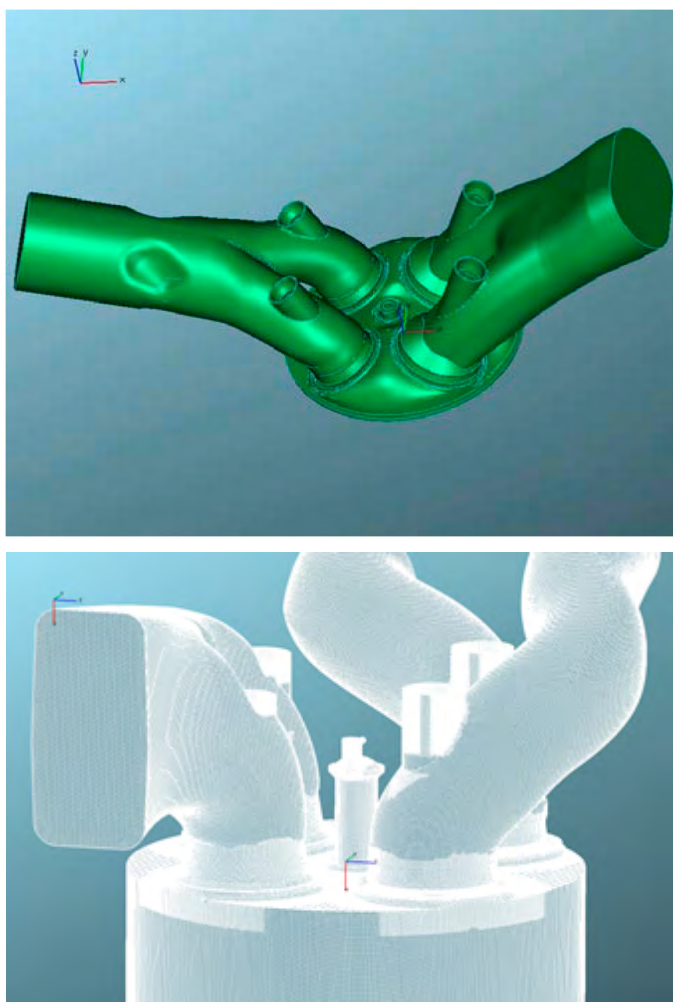


FIGURE 3: 3-D CAD geometries of considered engine cases (Table 1 and 2) – the Engine A (upper subfigure) and the Engine B (lower subfigure).

OBRAZĚK 3: 3-D CAD geometrie uvažovaných motorů (tabulky 1 a 2) – varianta A (horní obrázek) a variant B (dolní obrázek).



TABLE 3: Considered operating conditions for both engine version (A and B).
TABULKA 3: Uvažované pracovní podmínky pro obě verze motoru (A a B).

Parameter	Unit	Engine A	Engine B
Engine Speed	[rpm]	2000 – 3000	1800
IMEP	[bar]	2.0 – 3.0	5 – 9
Air Excess	[1]	1.0 – 1.3	1.0 – 1.9
Residual Gas Content	[%]	10 – 30	< 10

Regarding the Engine A, the following operating conditions were considered: motored regimes (at different engine speeds) and combustion regimes (2 operating points at low IMEP level). Many consecutive cycles (at least 30) were calculated to obtain statistical convergence of important output parameters. More detailed information about the Engine A can be found in [5, 6, 7].

Dealing with the Engine B, 3 different operating points were considered – these differ in air excess (un-throttled operation) ranging between 1.0 and 1.9 while engine speed was kept constant. Due to much more time demanding calculations (c.f. mesh parameters in Table 2), only 5 consecutive engine cycles were calculated. However, this should provide a good estimate of statistical moments of the 1st order (e.g., average values of scalar properties) – this observation is based on results from EU FP7 project LESSCCV, c.f. [7, 5]. More detailed information about the Engine B can be found in [16, 17].

There is additional significant difference between those selected engine cases – the Engine A represents a modern automotive SI DI ICE dominated by tumble while using classical ignition device (spark plug). On the other hand, the Engine B corresponds to gas SI ICE dominated by swirl, which is equipped with scavenged pre-chamber to be able to ignite very lean mixtures (hence, a turbulent flame jet ignition device is applied). The combustion process of the Engine A is a classical turbulent deflagration flame which has approximately spherical shape. Even though the combustion process in the Engine B is also a turbulent deflagration flame, its shape is dominated by turbulent flame jet shape, hence it is (in terms of its shape and time evolution) similar to combustion in CI (diesel) ICE.

4. MODEL CALIBRATION

Every calibration process requires reference data. In this case, these data were represented by experimental data typically measured at ICE test beds. This mainly includes in-cylinder pressure. Typically, more than 100 consecutive cycles (for each operating point) were measured and processed, hence both average cycle data and all individual cycle data were available. When calibrating 0-D/1-D models created in the tools [23, 24],

much more information was needed. However, when calibrating 3-D CFD models, in-cylinder pressure traces were sufficient. If any additional information was needed, it was transferred from the calibrated 0-D/1-D models (representing the ‘system level’ thermodynamic models) of the target engines.

Every model needs a calibration to match experimental data – this also applies to 3-D CFD modelling as well. However, the amount of model constants to be tuned is limited as these kinds of models are supposed to have high predictive ability, hence less tuning is necessary. In the above-mentioned case of LES ECFM-3Z model, there are 2 constants to be tuned: stretch factor and initial flame surfaces density (c.f. [22] for more details). The latter one (initial flame surface density) has relatively low influence and it is also related to initial parameters of flame kernel to be imposed to start the flame propagation process. On the other hand, the influence of stretch factor is very strong as it is shown in Figure 4. This parameter directly influences the speed in which the flame propagates, hence the higher the value, the faster the combustion process. In the presented cases (the Engine A and the Engine B – c.f. Table 1 and 2), the value of stretch factor was adjusted to match experimental data (pressure traces) for a selected operating conditions (e.g., engine speed and load). After that, it was fixed and kept constant for any other operating conditions of the selected engine case. Hence, the value is supposed to be engine specific. The value of initial flame surface density was estimated using recommended values from manual documentation of [22]. There is still one parameter to be adjusted, namely the phasing of combustion. As the way to initiate the flame propagation process is a bit artificial (prescribing flame kernel of certain size for certain time), the time does not correspond to a real ignition event. The empirical experience shows that flame initialization has to be timed few degrees of crank angle before the real ignition event. This timing adjustment has to be done for every engine operating point. On the other hand, both the stretch factor and the initial flame surface density are constant regardless of engine speed and/or load.

The quality of calibration process can be observed in Figure 9 for the Engine A and Figure 11 for the Engine B. Especially in the case of the Engine B the prediction is very good terms of combustion duration and CCV effects. In the case of the Engine A, there is good correspondence in terms of combustion duration, however CCV effects are a bit under-predicted. It should be stressed that even though both engine cases correspond to SI ICE concept, there is a fundamental difference between these engines in terms of flame topology. In the case of the Engine A, it is a classical SI ICE spherical flame (c.f. Figure 7). On the other hand, the Engine B is equipped with scavenged pre-chamber (it is a turbulent flame jet in terms of ignition device definition), which leads to very different flame



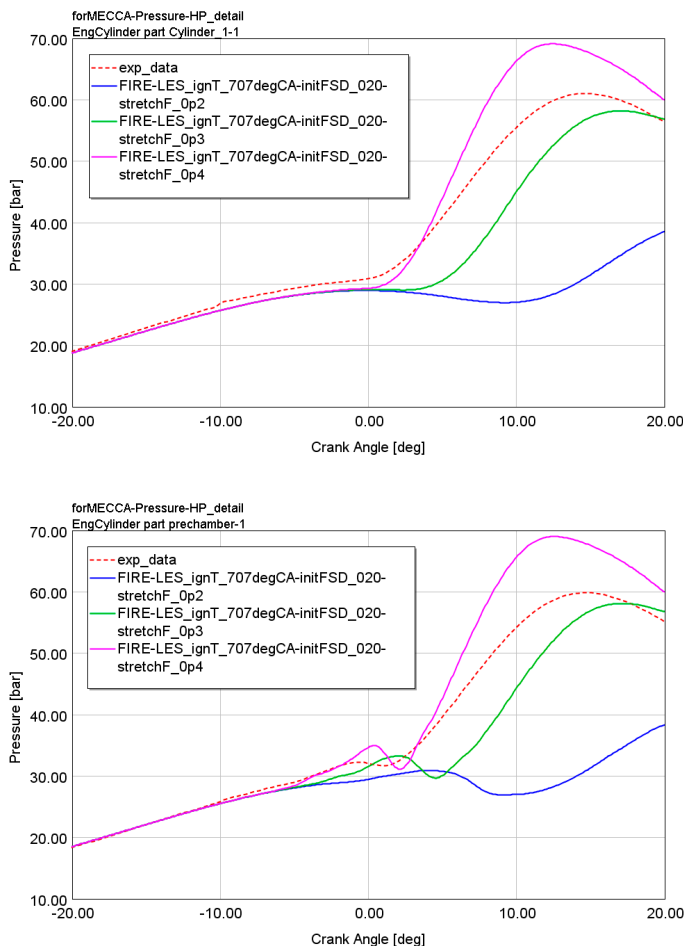


FIGURE 4: Tuning of combustion model (the Engine B – c.f. Table 1 and 2) – the influence of the stretch factor (LES ECFM-3Z model; blue curve represents the value of stretch factor of 0.2, green one of 0.3 and purple one of 0.4) – in-cylinder pressure is plotted in upper subfigure while pre-chamber pressure is shown in lower subfigure.

OBRÁZEK 4: Kalibrace modelu spalování (motor verze B – více v tabulkách 1 a 2) – vliv parametru „stretch factor“ (LES ECFM-3Z; modrá křivka odpovídá hodnotě „stretch factor“ 0.2, zelená 0.3 a fialová 0.4) – horní obrázek zobrazuje tlak ve válci, zatímco dolní obrázek ukazuje tlak v komůrce.

structure – it is similar to diesel engines when observing the shape of burnt/unburnt zone (c.f. Figure 14). However, it is deflagration flame in both engine cases.

5. DISCUSSION OF RESULTS

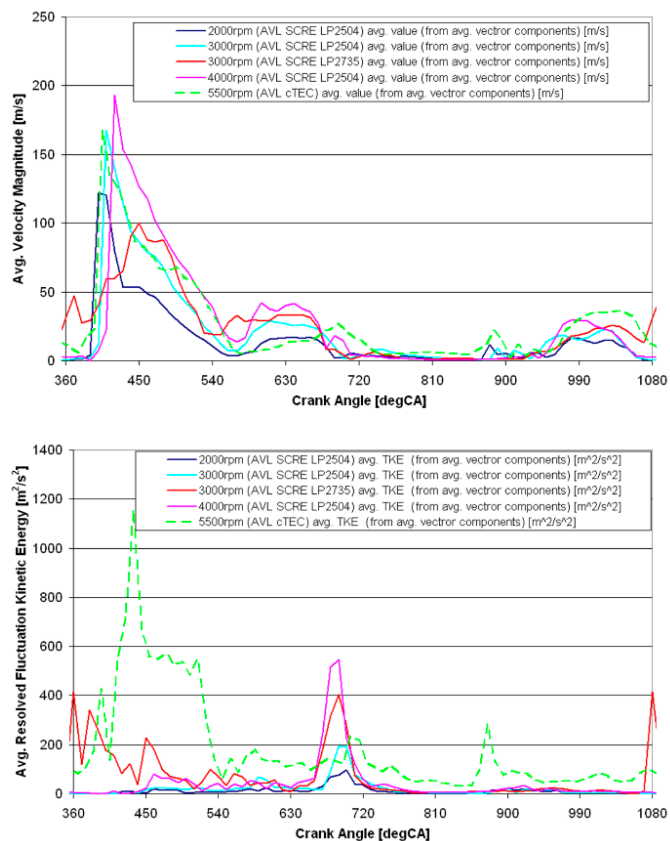
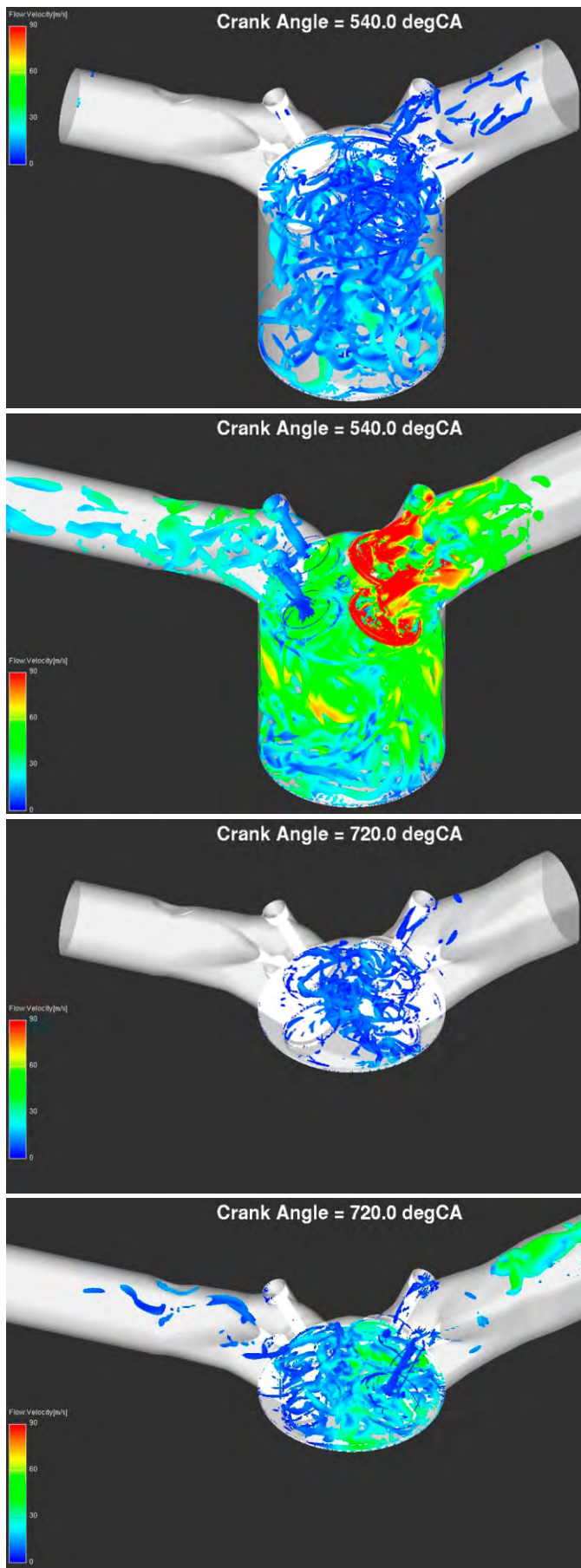
As it is mentioned above, the main focus of the paper is to study CCV effects by means of detailed 3-D CFD LES simulation approach. Two different engine cases were selected – the first one corresponds to a classical automotive direct injection SI ICE while the second one represents a scavenged pre-chamber concept applied to gas SI ICE. Many CFD data were obtained within past years dealing with these engine cases. The most relevant results in terms of CCV are presented in this section.

Strongly turbulent in-cylinder flow structure is shown in Figure 5 – the turbulence is generated during intake stroke while it decays during compression stroke. There are many parameters influencing this complex process – engine speed or intake valve timing are among the most important ones. These are well-known facts – c.f. [19]. Early flame kernel development is a critical phase of combustion process influencing subsequent phase of classical deflagration flame development. Even motored regimes show relatively strong CCV effects, which also applies to spark plug location – c.f. Figure 6. While average velocity strongly decreases during compression stroke, fluctuation component of velocity vector has relatively high peak just before TDC – this peak is positioned just in the typical window of ignition event. Hence, early flame kernel development is strongly influenced by that phenomenon, which subsequently influences both flame shape and its propagation – this is clearly seen in Figure 7. It seems that there is a correlation between resolved fluctuation kinetic energy (RFKE – the definition is presented in [21]; simply speaking, it is a difference between average total kinetic energy and kinetic energy based on average velocity vector – hence it represents the average value of kinetic energy of fluctuation velocity vector; however, this property consists of 2 major parts – turbulence and cycle-to-cycle variations; for low CCV cases, the latter one is usually neglected) peak at spark plug location (near TDC) and level of CCV – if the peak is significantly higher, early flame kernel development shows higher level of CCV which leads to high CCV of the whole combustion phase. Additional information about the term RFKE is presented in detail in paper [5] including its pattern for different cases.

Data presented in Figure 6, which represents motored operation of ICE, clearly indicate that main phenomenon behind CCV is the turbulent nature of the flow itself. The strong variability of velocity vector is mainly the outcome of intake stroke when strong tumble vortex is created. This large-scale structure is deformed (compressed) during the compression stroke. This leads to increase of its angular velocity, which in turn increases all dissipative processes. Hence, strong turbulence is created. As intake stroke (i.e., tumble vortex formation) already features relatively high level of CCV – c.f. Figure 8, it can be expected that this trend is preserved during compression stroke. Due to non-linear effects related to strong tumble dissipation near TDC, there is a peak of velocity vector fluctuation component (Figure 6). As there is little difference between motored operation of ICE and combustion one in terms of both intake stroke and compression one, the above mentioned statements are generally valid. These effects are further magnified when combustion process is started – c.f. Figure 7. This is mainly related to the nature of turbulent deflagration flame – more details can be found in [19, 20].

Results concerning combustion operation are shown in Figure 7, 9 and 10 for the Engine A and in Figure 11 and 14 for the





↑ **FIGURE 6:** Comparison of selected properties at spark plug location for different engine operating conditions (low CCV case, label 'LP2504' at 2000 rpm, is plotted in dark blue color; high CCV case, label 'LP2735' at 3000 rpm, is plotted in red color; more details can be found in [5, 6]) for motored regimes (engine speed is mentioned in figure legend; no throttling was applied) of the Engine A case (c.f. Table 1 and 2) – left subfigure represents magnitude of average velocity vector (based on more than 20 consecutive cycles) while right subfigure corresponds to resolved fluctuation kinetic energy.

OBRAZĚK 6: Porovnání vybraných veličin v místě svíčky pro různé pracovní body (bod s nízkou mezicyklovou variabilitou, označení „LP2504“ při 2000 otáčkách, je zobrazen tmavě modrou barvou; bod s vysokou má barvu červenou, označení „LP2735“ při 3000 otáčkách; více informací lze nalézt v [5, 6]) pro protáčené režimy motoru (otáčky motoru jsou zmíněny v legendě; bez škrcení) varianty A (více v tabulkách 1 a 2) – levý obrázek reprezentuje střední velikost vektoru rychlosti (založeno na minimálně 20 po sobě jdoucích cyklech), zatímco pravý obrázek odpovídá výpočtem zachycené kinetické energii fluktuací.

← **FIGURE 5:** Comparison of low CCV engine operating conditions (left column) and high CCV ones (right column) at different crank train positions (top row: BTD, bottom row: TDC) for the Engine A case (c.f. Table 1 and 2) – iso-surface of constant Q-invariant; the property mapped on the iso-surface is velocity vector magnitude (red color corresponds to 90 m/s; blue one represents 0 m/s).

OBRAZĚK 5: Porovnání pracovního bodu s nízkou mezicyklovou variabilitou (levý sloupec) a vysokou (pravý sloupec) v různých polohách klikového mechanismu (horní řádek: dolní úvrať, dolní řádek: horní úvrať) pro motor varianty A (více v tabulkách 1 a 2) – izoplocha konstantní hodnoty Q-invariantu; barva odpovídá hodnotě velikosti vektoru rychlosti (červená barva odpovídá 90 m/s, modrá 0 m/s).



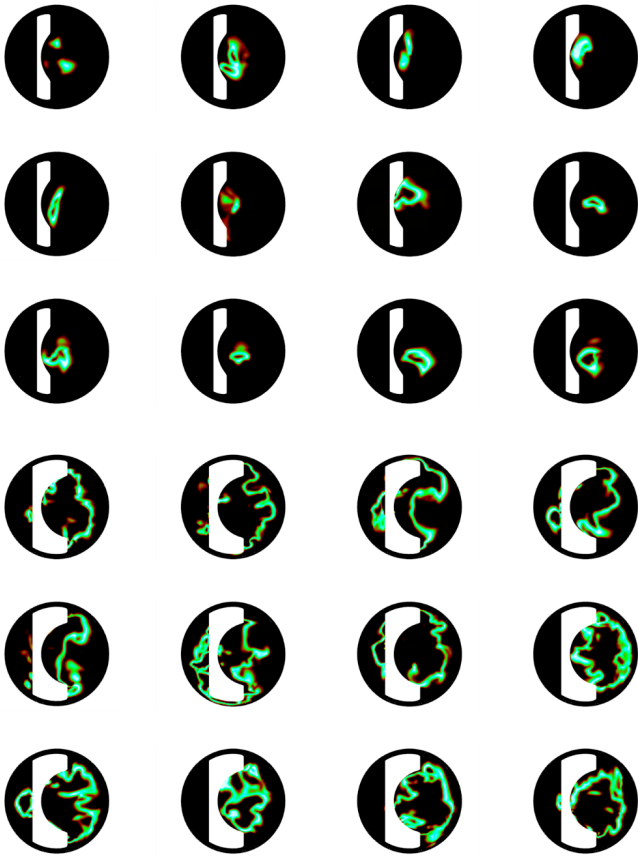


FIGURE 7: Flame front position (12 consecutive cycles are shown) for high CCV operating conditions at different combustion phases for the case of the Engine A (c.f. Table 1 and 2), top view – top subfigure (consisting of 12 sub-subfigures) corresponds to early combustion phase while bottom one (again consisting of 12 sub-subfigures) represents main combustion phase (rapid burning phase); green color represents burning zone.

OBRÁZEK 7: Poloha fronty plamene (zobrazeno je 12 po sobě následujících cyklů) pro pracovní bod s vysokou mezicyklovou variabilitou během různých fází hoření pro motor varianty A (více v tabulkách 1 a 2), pohled shora – horní obrázek (skládající se z 12 dalších obrázků) odpovídá úvodní fázi spalování, zatímco dolní (opět skládající se z 12 dalších obrázků) reprezentuje hlavní fázi hoření; zelená barva odpovídá hořící zóně.

Engine B. Regarding the pressure traces of the Engine A case (Figure 9), the influence of very early combustion phase (flame kernel development) can be quantified. The left subfigure of Figure 9 corresponds to setting when flame initialization was kept constant – hence, only turbulence effects are responsible for CCV of pressure traces. It can be seen that scatter of pressure traces is relatively low when compared with experimental data. The right subfigure represents setting when certain level of flame initialization variation was imposed (the value of initial flame surface density was randomly varied within certain interval, which was estimated by experts from AVL). It can be observed that CCV of pressure traces was increased and there is a better correspondence between prediction and experimental data. Hence, it confirms that there is a significant influence of

early flame kernel development on combustion process and that early flame kernel development features CCV effects as well – it is assumed that this is a consequence of local thermodynamic properties at spark plug, which vary strongly (c.f. Figure 6). These results are in-line with conclusions from [18], which are based on statistical analysis of experimental data and simulations based on 0-D/1-D approach.

Figure 10 shows CCV effects of ROHR (left subfigure) and global (in-cylinder average) air excess (right subfigure). Engine is operated in slightly lean conditions for this case. Significant variation of both ROHR and global air excess can be observed. Strong air excess variations are mainly due to high valve overlap, hence there is high internal EGR which varies a lot among cycles – that is why air excess is also varied strongly. It can be shown that in-cylinder flow during intake stroke (in terms of total fresh mixture in-flow) is almost constant for all the cycles, hence it is not the main source of air excess CCV. More information can be found in [5, 6].

On the other hand, combustion in the Engine B is different – based on [19], its ignition system can be labelled as turbulent flame jet, which can be clearly seen in Figure 14. Even though it is SI engine dominated by deflagration flame propagation, the flame topology is different when compared with classical spherical flame of SI ICE (compare Figure 7 with Figure 14). Regarding CCV effects, the prediction matches experimental data well – c.f. Figure 11 – without a need to impose variation of early flame kernel development phase. There are multiple reasons behind that statement. First, the mesh is significantly finer (c.f. Table 2), hence resolved turbulence is finer as well, which leads to lower requirement for additional modelling. Second, the combustion is mainly dominated by turbulent flame jet during early phase of in-cylinder combustion process – the jet is relatively strong, which leads to fast in-cylinder combustion. Third, the turbulent flame jet is primarily driven by pressure difference between pre-chamber and cylinder, which is relatively similar when comparing different engine cycles – it seems that this phenomenon leads to dampening of CCV effects taking place in pre-chamber. Based on all these facts, early flame kernel development phase (taking place in pre-chamber) seems to have a lower influence on CCV. Cyclic variation is mainly dominated by turbulent flame jet development – this also includes its timing, which is slightly different among the cycles due to different pre-chamber combustion duration (c.f. Figure 12 and Figure 13).

Combustion progress in a cylinder of the Engine B is shown in Figure 12. Unlike in the case of the Engine A (c.f. Figure 9), its shape seems to be similar for all calculated cycles while the main difference is combustion timing. Initial phase of in-cylinder combustion is primarily influenced by turbulent flame jet, the timing of which corresponds to combustion progress in a pre-chamber – in other words: in-cylinder combustion starts only



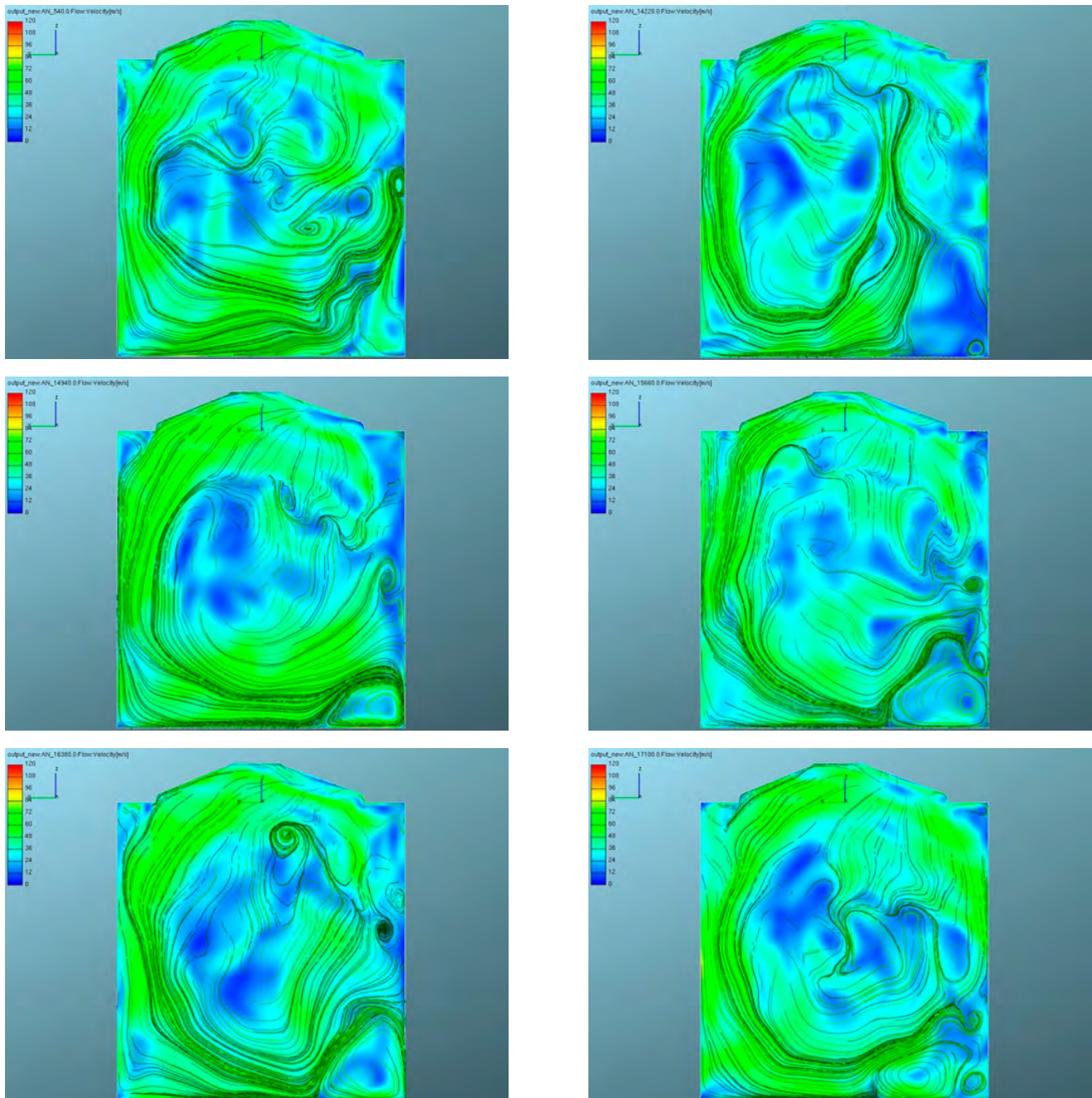


FIGURE 8: Tumble vortex structure at the end of intake stroke for the case of the Engine A (c.f. Table 1 and 2) – velocity vector magnitude is plotted (blue color represent the value of 0 m/s, red one corresponds to 120 m/s), black color curves represent streamlines; six consecutive engine cycles are shown.

OBRÁZEK 8: Struktura příčného víru (tumble) na konci sacího zdvihu pro motor varianty A (více v tabulkách 1 a 2) – je zobrazena velikost vektoru rychlosti (modrá barva reprezentuje 0 m/s, červená 120 m/s), černé křivky jsou proudnice; je zobrazeno 6 po sobě následujících cyklů.

when turbulent flame jet is initiated due to flame front reaching connecting channels between a pre-chamber and a cylinder. The early phase of in-cylinder combustion seems to be nearly identical in terms of rate of heat release (c.f. Figure 12) – up to approx. 30% of burnt fuel, the slope of ROHR curve (left subfigure in Figure 12) is almost the same for all calculated cycles. This suggests that early in-cylinder flame development, which is mainly dominated

by turbulent flame jet, is little dependent on instantaneous local thermodynamic status in both pre-chamber and cylinder. Hence, any local differences due to CCV effects (when comparing different cycles) are suppressed. Any visible CCV effects (in terms of ROHR) are developed only at later phases of combustion process as turbulence needs some time to develop local differences, which lead to different rate of heat release.



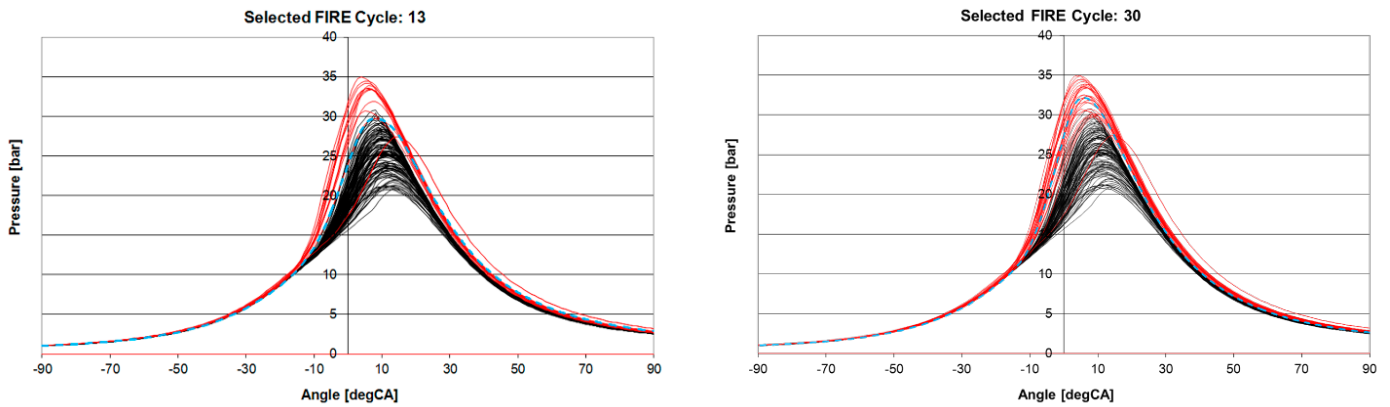


FIGURE 9: Comparison of individual cycle pressure traces between simulation (red color) and experimental data (black color) for high CCV operating conditions for the case of the Engine A (c.f. Table 1 and 2) – left subfigure corresponds to constant setting of ignition model while right subfigure represents a random variation of ignition model setting (initial value of Flame Surface Density of LES ECFM-3Z model).

OBRÁZEK 9: Porovnání tlaků ve válci pro jednotlivé cykly mezi simulací (červená barva) a experimentálními daty (černá barva) pro pracovní bod s vysokou mezicyklovou variabilitou pro motor varianty A (více v tabulkách 1 a 2) – levý obrázek odpovídá konstantnímu nastavení modelu pro zážeh, zatímco pravý obrázek reprezentuje náhodné variace modelu zážehu (počáteční hodnota pro FSD modelu LES ECFM-3Z).

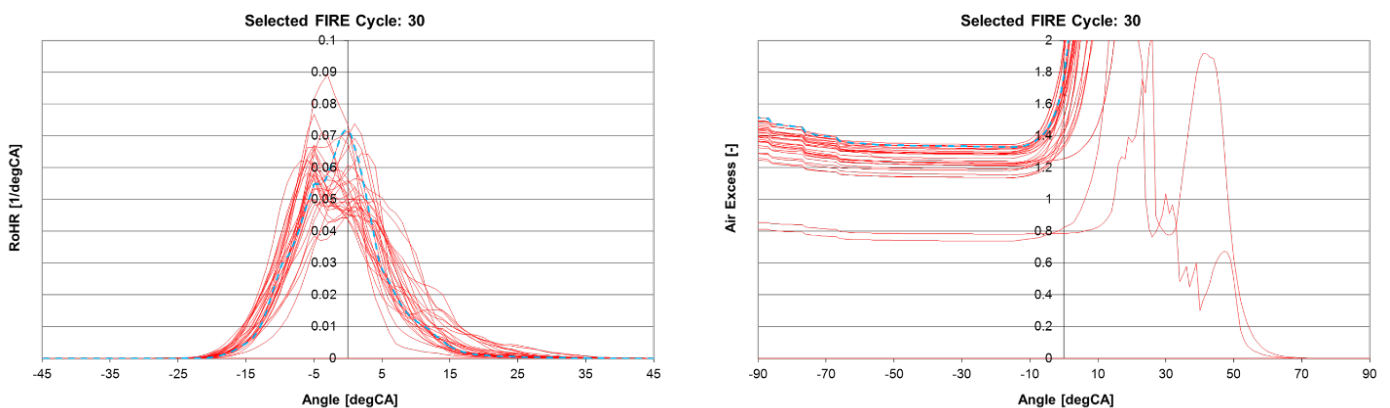


FIGURE 10: Comparison of individual cycle data from simulation for high CCV operating conditions for the case of the Engine A (c.f. Table 1 and 2) – left subfigure corresponds to normalized rate of heat release (ROHR) while right subfigure represents instantaneous mean in-cylinder air excess.

OBRÁZEK 10: Porovnání dat ze simulací pro jednotlivé cykly pro pracovní bod s vysokou mezicyklovou variabilitou pro motor varianty A (více v tabulkách 1 a 2) – levý obrázek odpovídá normalizované rychlosti vývinu tepla, zatímco pravý obrázek reprezentuje okamžitý střední přebytek vzduchu.

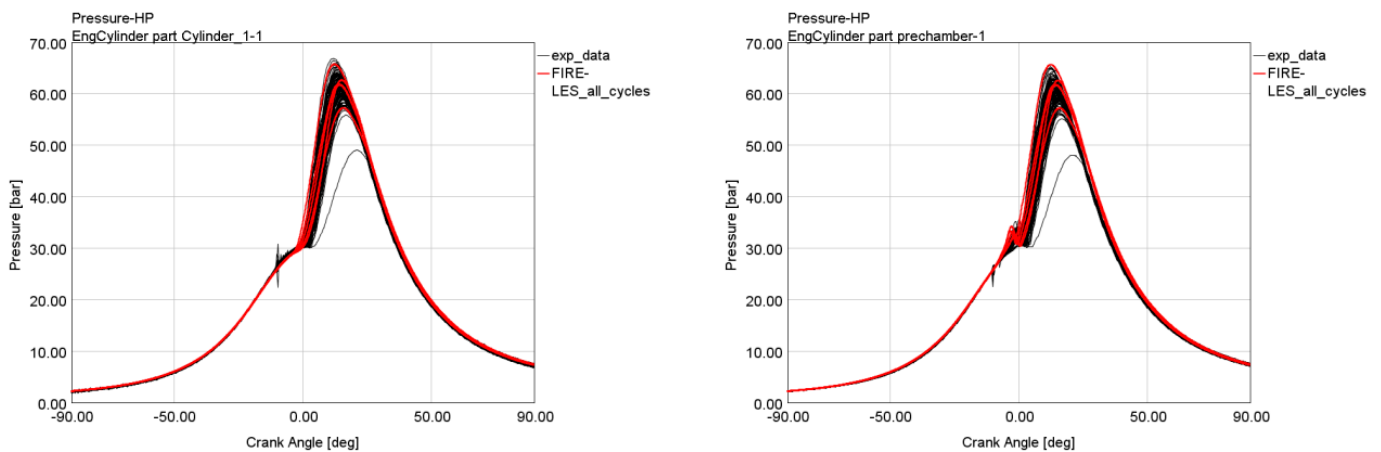


FIGURE 11: Comparison of individual cycle pressure traces between simulation (red color) and experimental data (black color) for the stoichiometric operation for the case of the Engine B (c.f. Table 1 and 2) – left subfigure corresponds to in-cylinder pressure while right subfigure represents pressure in pre-chamber.

OBRÁZEK 11: Porovnání tlaků ve válci/komůrce pro jednotlivé cykly mezi simulací (červená barva) a experimentálními daty (černá barva) pro pracovní bod se stechiometrickou směsí pro motor varianty B (více v tabulkách 1 a 2) – levý obrázek odpovídá tlaku ve válci, zatímco pravý obrázek reprezentuje tlak v komůrce.



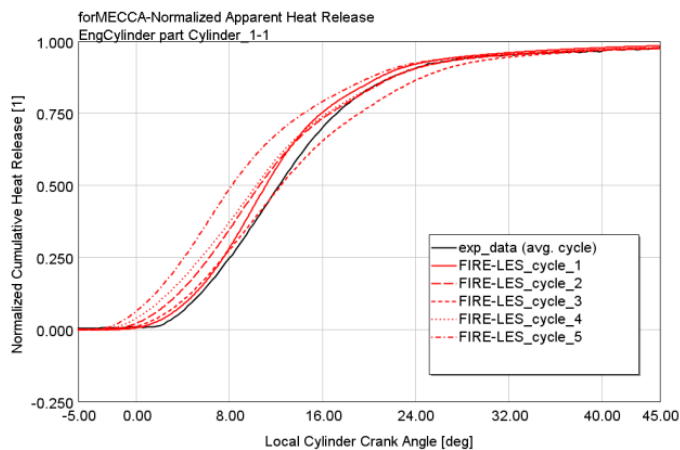
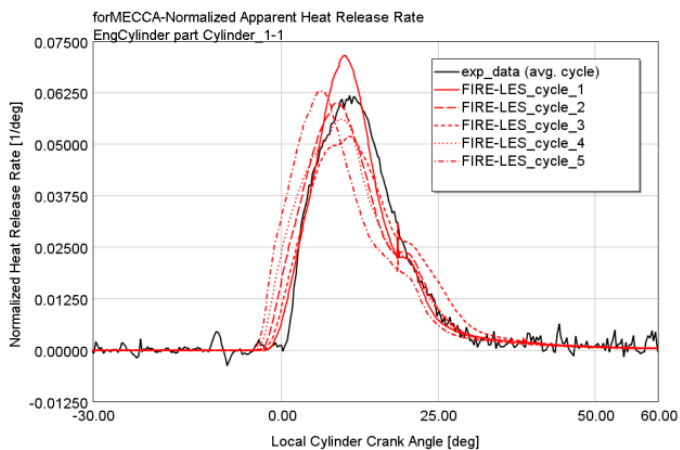


FIGURE 12: Comparison of individual cycle simulation data related to combustion (red color) and experimental data (black color; average cycle) for the stoichiometric operation for the case of the Engine B (c.f. Table 1 and 2) – left subfigure corresponds to normalized in-cylinder rate of heat release (ROHR) while right subfigure represents normalized in-cylinder heat release.

OBRÁZEK 12: Porovnání dat ze simulací pro jednotlivé cykly (červená barva) a experimentálních dat (černá barva; průměrný cyklus) pro pracovní bod se stechiometrickou směsí pro motor varianty B (více v tabulkách 1 a 2) – levý obrázek odpovídá normalizované rychlosti vývinu tepla ve válci, zatímco pravý obrázek reprezentuje normalizovaný vývin tepla ve válci.

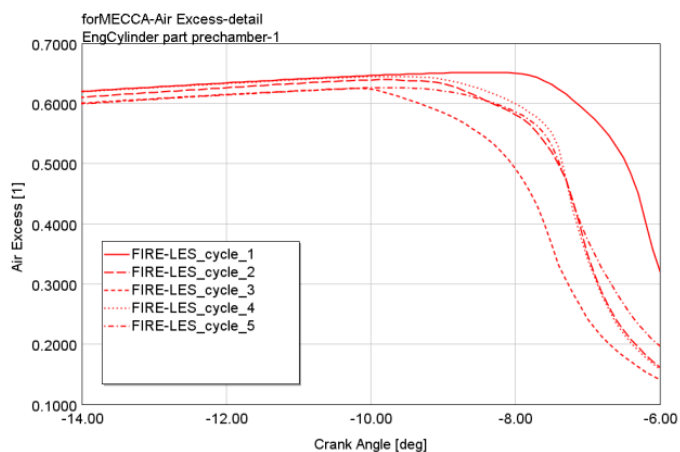
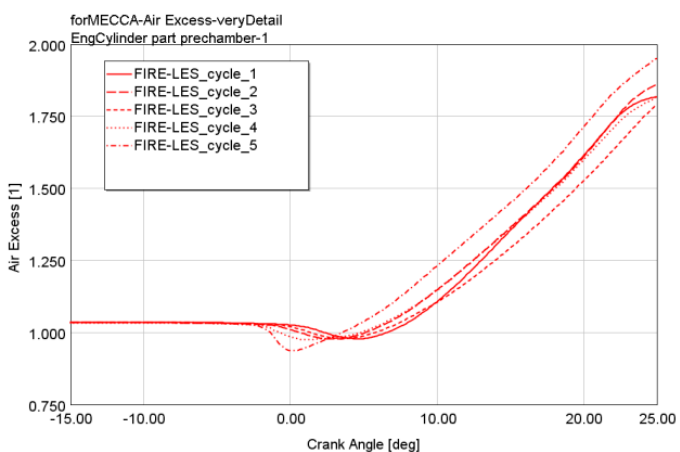


FIGURE 13: Comparison of individual cycle simulation data related to combustion (red color) for the stoichiometric operation for the case of the Engine B (c.f. Table 1 and 2) – left subfigure corresponds to mean in-cylinder air excess while right subfigure represents mean pre-chamber air excess (spark timing is set to -11 degCA).

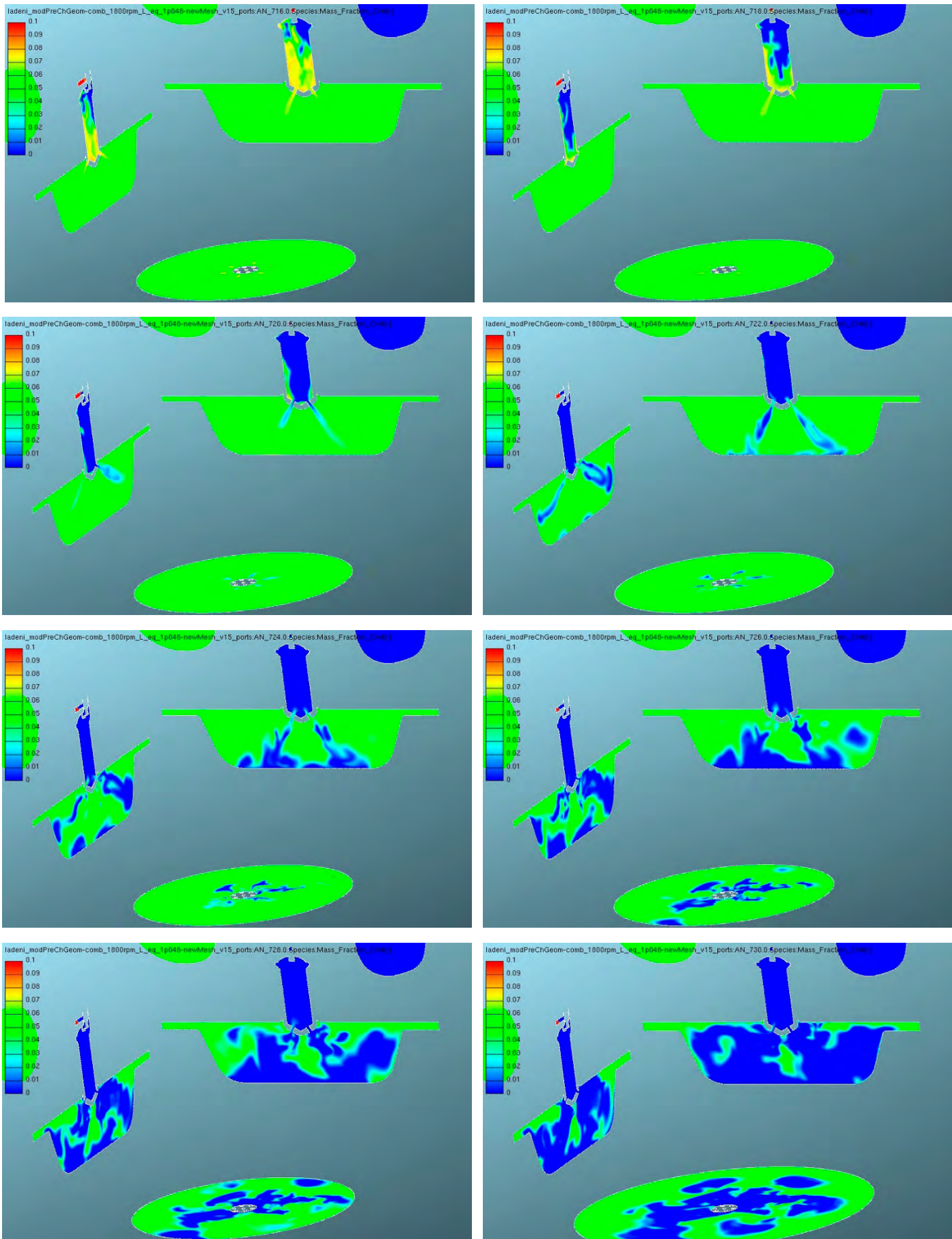
OBRÁZEK 13: Porovnání dat ze simulací pro jednotlivé cykly (červená barva) pro pracovní bod se stechiometrickou směsí pro motor varianty B (více v tabulkách 1 a 2) – levý obrázek odpovídá prostorově střednímu přebytku vzduchu ve válci motoru, zatímco pravý obrázek reprezentuje střední přebytku vzduchu v komůrce (přeskok jiskry nastává při -11° pootočení klikového mechanismu).

The above mentioned phenomena are confirmed in Figure 13 – global mean air excess is shown for different cycles. There is relatively low CCV of pre-chamber mean air excess (right subfigure of Figure 13). However, visible start of pre-chamber combustion process (detected by strong decrease of mean air excess in Figure 13) varies within 3 degCA. It seems that pre-chamber flame front progress is similar for all calculated cycles, hence it reaches connecting channels at different crank angle positions (when comparing different engine cycles). Start of in-cylinder combustion is related to small decrease of mean in-cylinder air excess due to the fact that relatively high amount

FIGURE 14: Flame development in time domain for the case of the Engine B (c.f. Table 1 and 2) – fuel mass fraction is plotted (blue color represents burnt zone); top left subfigure corresponds to 716 degCA, all other sub-figures represent increase by 2 degCA (red color corresponds to 0.1 CH4 mass fraction; blue one represents 0).

OBRÁZEK 14: Postup plamene v čase pro motor varianty B (více v tabulkách 1 a 2) – je zobrazen hmotnostní podíl paliva (modrá barva reprezentuje spálenou zónu); levý horní obrázek odpovídá 716° natočení klikového hřídele, každý další obrázek reprezentuje nárůst o 2° (červená barva odpovídá 0.1 hmotnostního podílu CH4, modrá 0).





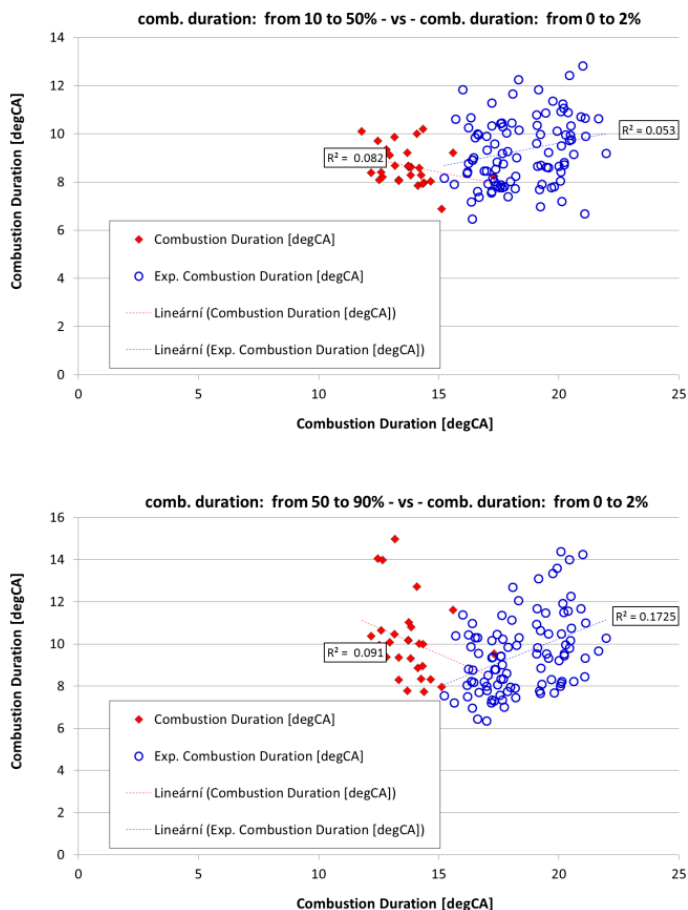


FIGURE 15: Comparison of individual cycle data between simulation (red color) and experimental data (blue color) for high CCV operating conditions for the case of the Engine A (c.f. Table 1 and 2) – left subfigure corresponds to correlation between early combustion phase duration (from 0 to 2% of burnt fuel) and first part of rapid combustion phase (from 10 to 50% of burnt fuel) while right subfigure represents correlation between early combustion phase duration and second part of rapid combustion phase (from 50 to 90% of burnt fuel).

OBRÁZEK 15: Porovnání dat pro jednotlivé cykly mezi simulací (červená barva) a experimentálními daty (modrá barva) pro pracovní bod s vysokou mezicyklovou variabilitou pro motor varianty A (více v tabulkách 1 a 2) – levý obrázek odpovídá korelaci mezi úvodní fází spalování (od 0 do 2% spáleného paliva) a první částí hlavní fáze spalování (od 10 do 50% spáleného paliva), zatímco pravý obrázek reprezentuje korelaci mezi úvodní fází spalování a druhou částí hlavní fáze spalování (od 50 do 90% spáleného paliva).

of pre-chamber mixtures is pushed out of pre-chamber by increased pressure in a pre-chamber – this decreases mean air excess in a cylinder as pre-chamber mixture is rich. After that, combustion progress is similar for all considered cycles, hence confirming the data from Figure 12. This analysis suggests that pre-chamber combustion system is less sensitive to CCV effects – this is a consequence of turbulent flame jet phase which seems to dampen/suppress influence of local thermodynamic CCV. Details of combustion process in the Engine B are shown in Figure 14. Combustion in pre-chamber is similar to combustion

in classical SI engine, however mixture homogeneity CCV is higher – this is mainly related to swirling motion in pre-chamber coupled with small connecting channels. This phase is relatively slow. Once the flame reaches connecting channels (between pre-chamber and cylinder), there is relatively high pressure drop (i.e., pre-chamber pressure is clearly higher than in-cylinder pressure), which leads to high flame jet velocities (reaching values up to 200 m/s). Hence, flame jet reaches outer boundaries (e.g., piston top crown) very fast – this typically takes 2 degCA. After that, a complicated turbulent flame structure is being developed as a consequence of swirling in-cylinder motion and interaction among 12 turbulent flame jets. All that leads to fast combustion – in the case shown in Figure 14, it takes cca 10 degCA to burn all the mixture in the piston bowl. The qualitatively same effects are observed even for cases of very lean mixture combustion. Hence, it confirms that turbulence is dominating the initial phase of combustion (i.e., up to the point of 30% of burnt fuel).

Comparison of selected integral data between LES prediction and measurement is shown in Figure 15. It corresponds to different combustion phase durations. As it is clear from this figure, LES simulation is capable of reasonably good prediction – this concerns both qualitative trends (the shape of data set) and quantitative data (CCV). Other important information (based on Figure 15) is that there is very weak correlation among shown parameters, hence supporting (to a certain extent) the idea presented in some literature sources that CCV is a random process. Similar diagrams can be shown for other important cycle-specific ICE parameters (e.g., internal EGR, air excess, IMEP, max. in-cylinder pressure).

Based on above mentioned and Figure 15, it is clear that it is very difficult to predict future development within a single engine cycle while using statistical approach – the reason behind that is that correlations are very weak. This leads to conclusion that previous cycle history has to have even lower influence on combustion development during the subsequent cycle. This conclusion is clearly confirmed in [18] where experimental data are analyzed.

6. CONCLUSION

The presented paper deals with identification of main sources of cycle-to-cycle variations (CCV) in SI ICE. The main approach to achieve this target is based on 3-D CFD simulations while using LES. Two different engine cases were studied – the first one corresponds to modern automotive DI SI ICE dominated by tumble in-cylinder vortex, the second one represents gas SI ICE equipped with scavenged pre-chamber while in-cylinder flow is dominated by swirl.



In-cylinder turbulence was identified as the main source of CCV – this is in-line with well-established knowledge of SI ICE operation. The detailed 3-D CFD LES simulations confirm that the turbulence, which is created mainly during intake stroke while being strongly dissipated during compression stroke, is responsible for significant local differences of important thermodynamic properties (from CCV point of view). These are magnified by deflagration flame front propagation, the nature of which is strongly dependent on local turbulence. This also confirms the fact that the history of previous cycle(s) has almost no influence on combustion process of the current cycle. Moreover, combustion progress integral data correlations are very weak, hence it is very difficult to statistically estimate future development even if certain information from current cycle is known. This may support (to a certain extent) the idea presented in some literature sources that CCV is a random process – sometimes the following term is used to describe complex in-cylinder phenomena: ‘organized chaos’.

Other important CCV source is the very beginning of combustion process – the early flame kernel development phase. This is difficult to predict in CFD without special detailed complex sub-models taking into account electro-magnetic phenomena and chemical ones as well. The prove of its importance was achieved indirectly – sensitivity studies were carried out to show that certain CCV level (of early flame kernel development process) has to be imposed to achieve experimentally observed CCV of pressure traces. These conclusions are also confirmed by the work presented in [18]. This CCV source is less important than turbulence, however its non-linear interaction with local turbulence leads to strong CCV effects.

Two different ignition systems were compared: the classical spark ignition one and turbulent flame jet one. Analysis of the data suggests that the latter one is less prone to magnify any CCV caused by ignition event. The main reason behind that statement is the fact that turbulent flame jet, which ignites the mixture in main cylinder of ICE, is primarily dependent on pressure difference (between pre-chamber and cylinder). Hence any local differences due to turbulence in pre-chamber have less influence on flame development in the main cylinder. Additional observation is that the flame structure of pre-chamber SI ICE is very different to a classic spherical flame front of a typical SI ICE – its topology is similar to diesel combustion in CI ICE. Moreover, the combustion is very fast in a main cylinder even when very lean mixture is used.

The 3-D CFD approach based on LES has proved to be an efficient and reliable tool when dealing with CCV effects – this was shown within EU FP7 project LESSCCV and it was confirmed by work presented in this paper as well. It can predict qualitative trends correctly while quality of quantitative predictions is usually fine.

ACKNOWLEDGEMENTS

This research has been realized using the support of Technological Agency, Czech Republic, program Centres of Competence, project TE01020020: ‘Josef Božek Competence Centre for Automotive Industry’.

This research has been realized using the support of EU Regional Development Fund in OP R&D for Innovations (OP VaVpl) and The Ministry of Education, Youth and Sports, Czech Republic, project CZ.1.05/2.1.00/03.0125: ‘Acquisition of Technology for Vehicle Center of Sustainable Mobility’.

This research has been realized using the support of The Ministry of Education, Youth and Sports program NPU I (LO), project LO1311: ‘Development of Vehicle Centre of Sustainable Mobility’.

All the help has been gratefully appreciated.

LIST OF NOTATIONS AND ABBREVIATIONS

BTD	Bottom Dead Centre
CCV	Cycle-to-Cycle Variation(s)
CFD	Computational Fluid Dynamics
CI	Compression Ignition
COV	Coefficient of Variation
DI	Direct Injection
ECFM-3Z	Extended Coherent Flamelet Model – 3-zone version
EGR	Exhaust Gas Recirculation
FSD	Flame Surface Density
IMEP	Indicated Mean Effective Pressure
ICE	Internal Combustion Engine
IVC	Intake Valve Closing
KE	Kinetic Energy
LES	Large Eddy Simulation
PDF	Probability Density Function
PFI	Port Fuel Injection
RANS	Reynolds Averaged Navier-Stokes (equation set)
RFKE	Resolved Fluctuation Kinetic Energy
ROHR	Rate of Heat Release
SI	Spark Ignition
SW	Software
TKE	Turbulence Kinetic Energy
TDC	Top Dead Centre



REFERENCES

- [1] Moureau, V., Barton, I., Angelberger, C., Poinso, T., 2004. *Towards Large Eddy Simulation in Internal-Combustion Engines: Simulation of a Compressed Tumble Flow*, SAE Technical Paper 2004-01-1995, 2004, doi: 10.4271/2004-01-1995.
- [2] Vermorel, O., Richard, S., Colin, O., Angelberger, C., Benkenida, A., Veynante, D., 2007. *Multi-Cycle LES Simulations of Flow and Combustion in a PFI SI 4-Valve Production Engine*, SAE Technical Paper 2007-01-0151, 2011, doi: 10.4271/2007-01-0151.
- [3] Pera, C., Angelberger, C., 2011. *Large Eddy Simulation of a Motored Single-Cylinder Engine Using System Simulation to Define Boundary Conditions: Methodology and Validation*, SAE Int. J. Engines 4(1):948-963, doi: 10.4271/2011-01-0834.
- [4] Thobois, L., Rymer, G., Soulères, T., Poinso, T., 2004. *Large-Eddy Simulation in IC Engine Geometries*, SAE Technical Paper 2004-01-1854, 2004, doi:10.4271/2004-01-1854.
- [5] Vitek, O., Macek, J., Tatschl, R., Pavlovic, Z. et al., 2012. *LES Simulation of Direct Injection SI-Engine In-Cylinder Flow*, SAE Technical Paper 2012-01-0138, <https://doi.org/10.4271/2012-01-0138>.
- [6] Tatschl, R., Bogensperger, M., Pavlovic, Z., Priesching, P. et al., 2013. *LES Simulation of Flame Propagation in a Direct-Injection SI-Engine to Identify the Causes of Cycle-to-Cycle Combustion Variations*, SAE Technical Paper 2013-01-1084, <https://doi.org/10.4271/2013-01-1084>.
- [7] Vitek, O., Macek, J., Pavlovic, Z., et al., 2016. *Statistical Analysis of Detailed 3-D CFD LES Simulations with Regard to CCV Modeling*, Journal of Middle European Construction and Design of Cars, 14(1), pp. 1-16. doi:10.1515/meccdc-2016-0001
- [8] R. Issa, 1991. *Solution of the Implicitly Discretized Fluid Flow Equations by Operator-splitting*, In Journal of Computational Physics, Volume 62, Issue 1, 1986, Pages 40-65, ISSN 0021-9991, [https://doi.org/10.1016/0021-9991\(86\)90099-9](https://doi.org/10.1016/0021-9991(86)90099-9).
- [9] Lesieur, M., Métais, O., Comte, P., 2005. *Large-Eddy Simulations of Turbulence*, Cambridge: Cambridge University Press, 2005. doi:10.1017/CBO9780511755507.
- [10] Smagorinsky, J., 1963. *General Circulation Experiments with the Primitive Equations*, Mon. Weather Rev., Vol. 91(3): 99-164
- [11] Hiromichi Kobayashi, 2005. *The Subgrid-scale Models Based on Coherent Structures for Rotating Homogeneous Turbulence and Turbulent Channel Flow*, Physics of Fluids, 17, 045104.
- [12] Hiromichi Kobayashi, Hama, F. and Wu, X., 2008. *Application of a Local SGS Model Based on Coherent Structures to Complex Geometries*, International Journal of Heat and Fluid Flow 29 640-653.
- [13] Richard S., Colin O., Vermorel O., Benkenida A., Angelberger C. and Veynante D., 2007. *Towards Large Eddy Simulation of Combustion in Spark Ignition Engines*, Proceedings of the Combustion Institute, Vol. 31, No. 1, pp. 3059-3066.
- [14] Zeldovich, Y. B., Sadovnikov, P. Y. and Frank-Kamenetskii, D. A., 1947. *Oxidation of Nitrogen in Combustion*, Translation by M. Shelef, Academy of Sciences of USSR, Institute of Chemical Physics, Moscow-Leningrad.
- [15] Dukowicz, J.K., 1980. *Particle-Fluid Numerical Model for Liquid Sprays*, J. Comp. Physics, 35, 229-253.
- [16] Vávra, J., Syrovátka, Z., Takáts, M., Barrientos, E., 2016. *Scavenged Pre-chamber on a Gas Engine for Light Duty Truck*, ASME 2016 Internal Combustion Engine Fall Technical Conference, ICEF 2016, doi: 10.1115/ICEF20169423.
- [17] Syrovátka, Z., Takáts, M., and Vavra, J., 2007. *Analysis of Scavenged Pre-Chamber for Light Duty Truck Gas Engine*, SAE Technical Paper 2017-24-0095, 2017, doi:10.4271/2017-24-0095.
- [18] Vitek, O., Macek, J., Poetsch, C., Tatschl, R., 2013. *Modeling Cycle-to-Cycle Variations in 0-D/1-D Simulation by Means of Combustion Model Parameter Perturbations based on Statistics of Cycle-Resolved Data*, SAE Int. J. Engines, 6(2), doi: 10.4271/2013-01-1314.
- [19] Heywood, J. B., 1988. *Internal Combustion Engine Fundamentals*, McGraw-Hill series in mechanical engineering, printed in USA. McGraw-Hill. ISBN 0-07-028637-X.
- [20] Peters, N., 2000. *Turbulent Combustion*, The Press Syndicate of the University of Cambridge, The Pitt Building, Trumpington Street, Cambridge. ISBN 0-521-66082-3.
- [21] Vitek, O., Mareš, B., Macek, J., 2014. *Application of LES Turbulence Model to Motored 4-Stroke Internal Combustion Engine*, Colloquium Fluid Dynamics 2010, October 2013.
- [22] AVL AST (2014). FIRE Manual v2014, AVL List GmbH, Graz.
- [23] BOOST 2011SP1 [DVD]. AVL List GmbH, 2011.
- [24] GT-Power User's Manual, GT-Suite version 7.3. Gamma Technologies Inc., 2012.

